Simulation and Investigations of the Effect of Cutting Parameters on Chip Formation of Aluminium alloy 6061-T6

Adedeji. A. Kasali, Nurudeen. A. Raji, Fadipe.O. Lukman, Aderibigbe.O. Michael.

Lagos State University, P.M.B.1087 Apapa, Lagos.

kasali.adedeji@lasu.edu.ng

Abstract

In this paper, modelling and simulation of orthogonal metal cutting of Aluminium 6061-T6 is performed by finite element method using ANSYS 19.2 software. Effects of depth of cut, cutting speed and tool rake face angle on cutting variables such as cutting forces, chip morphology, temperature and stress distributions are investigated using the Johnson-Cook and Johnson-Cook damage models. Estimation of the influence and important process parameters such as cutting speed, depth of cut, feed and tool rake angle on the cutting forces, temperature and stress distributions in tool geometries design and optimising the cutting conditions for profitable manufacture of quality machined products. Finite element modelling and simulation becomes an important alternative tool; where experimental techniques will require expensive equipment and result in material wastage. This makes it possible to predict the variation of important cutting variables without carrying out any experiment.

Keywords: *Aluminium alloy 6061-T6 ANSYS, Cutting Parameters, Chip Formation, Finite Element Simulation,*

1. Introduction

Aluminium alloy 6061 is one of the most extensively used of the 6000 series of aluminium alloys [1]. It is a versatile heat treatable extruded alloy with medium to high strength capabilities. 6061 is a precipitation-hardened aluminium alloy, containing magnesium and silicon as its major alloying elements. Originally called "Alloy 61S", it was developed in 1935. It has good mechanical properties, exhibits good weld ability, and is very commonly extruded (second in popularity only to 6063). It is one of the most common alloys of aluminium for general-purpose use [2].

Machining processes produce required shapes by material removal from selected areas of the work piece [3]. Most machining is achieved by straining a local region of the work piece to fracture by the relative motion of the tool and the work piece [4]. Machining is often used to produce shapes with high dimensional tolerance, good surface finish and most times with complex geometry [5]. It is regarded as a secondary process because it is often carried out on work piece that was produced using a primary process like casting, hot rolling or forging [6]. A great variety of

machining processes and machining tools are available to be utilized according to the required shape and geometry.

2. Material properties

Table 1: Mechanical properties of Al 6061-T6

Density(**ρ**)	2703 Kg/m^3
Modulus of Elasticity	68.9 GPa
Poisson's ratio	0.33
Ultimate Tensile Strength	310 N/mm^2
Shear Modulus	26 GPa
Tensile Yield strength	276 N/mm^2

Table 2: Composition of aluminium 6061-T6 [8]

Element	**Minimum weight (%)**	**Maximum weight (%)**
Silicon	0.4	0.8
Iron	-	0.7
Copper	0.15	0.4
Manganese	-	0.15
Magnesium	0.8	1.2
Chromium	0.04	0.35
Zinc	-	0.25
Titanium	-	0.15
Other Elements	0.05	0.15
Aluminium	95.85	98.56

3. Methodology

The effect of cutting parameters on the temperature, cutting and thrust forces, maximum residual stress and type of chip formed is discussed using the orthogonal cutting model by modelling and simulating the process on ANSYS 19.2 workbench. [14]

The parameters are:

- Cutting speed
- Depth of cut (which is the same as the feed rate in orthogonal cutting)
- Rake angle

A tungsten carbide cutting tool with width of cut 4mm was used in the orthogonal cutting of a rectangular Al 6061-T6 work piece of length 50mm, height 6mm and thickness 4mm.

The tool was modelled with three different rake angles -6°, 0° and 15° to observe the effect of the rake angle on the tool-work interface temperature, stress, cutting force and thrust force. All three tool models have a tool tip radius of 0.3mm and a clearance angle of 5°.

Three different depths of cut of 0.1mm, 0.2mm and 0.5mm were also used for all the three tool models created respectively.

The tool was modelled to travel across the entire length of the work piece at three different velocities; 50m/min, 150m/min and 250m/min which are the low, medium and high velocities respectively.

3.1. Johnson-Cook material model

Johnson and Cook (1993) [8] developed a material model based on torsion and dynamic Hopkinson bar test over a wide range of strain rates and temperatures. The Johnson-cook strength model was established as follows:

$$\sigma = (A + B\varepsilon^{n})\left(1 + C1n\frac{\dot{\varepsilon}}{\dot{\varepsilon}_0}\right)\left(1 - \left(\frac{T-T_r}{T_m-T_r}\right)^{m}\right) \quad (1)$$

The first term in parenthesis is the elastic-plastic term and it represents strain hardening. The second one is viscosity term and it shows that flow stress of material increases when material is exposed to high strain rates. The last one is the temperature softening term. A, B, C, n and m are material constants that are found by material tests. T is the instantaneous temperature, T_r is the room temperature and T_m is the melting temperature of a given material.

Table 3. J-C strength parameters for Aluminium 6061-T6 [7]

Initial Yield Stress, A (MPa)	Hardening Constant, B (MPa)	Hardening Exponent, C	Strain Rate Constant, n	Thermal Softening Exponent, m	Melting Temperature, T_m (°C)	Reference Strain Rate (/sec)
324	114	0.42	2.e-003	1.34	650	1

The Johnson-Cook failure model is based on a hypothesis that fracture occurs when the accumulated plastic strain reaches a critical value.

Table 4: J-C failure parameters for Aluminium 6061-T6 [7]

Damage Constant, D_1	Damage Constant, D_2	Damage Constant, D_3	Damage Constant, D_4	Damage Constant, D_5	Melting Temperature (°C)	Reference Strain Rate (/sec)
-0.77	1.45	-0.47	0	1.6	650	1

3.2. Modelling and simulation

The finite element mesh of tool is modelled using 4145 nodes and 19378 elements for the 15° rake tool, the -6° rake tool contained 6611 nodes and 31866 elements, while the 0° rake tool contained 4407 nodes and 20818 elements. Iso-parametric quadrilateral elements are used for the analysis. The mesh density of tool is modelled high to obtain more accurate temperature distribution results. The cutting tool was modelled as rigid while the work piece was defined as a flexible body connection

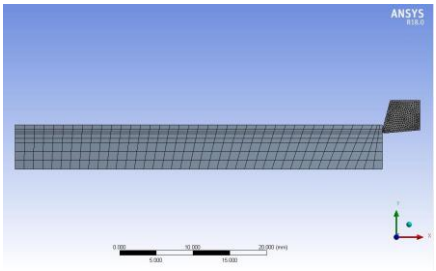

Fig 1. Mesh design of the rectangular workpiece and the 15° cutting tool

.

Table 5. Geometry Modelling variables of the cutting tool

Rake Angle, α (°)	Clearance/Relief Angle, θ (°)	Tip Radius, r_T (mm)
-6	5	0.3
0	5	0.3
15	5	0.3

Automatic contact regions were generated for the geometry assembly and the following contacts were defined between respective bodies and faces.

- The frictional contact was defined between the workpiece and aluminum alloy 6061 rectangular bar.

The rake face and the tool tip were assigned as target faces and the right end of the aluminum 6061 bar was assigned as the contact face.

- The contact type between the target and contact group was defined as frictional with a coefficient of friction of 0.5.

System modelling:

- Varying Initial velocity was given to the cutting tool in the X direction for different simulations.
- The workpiece is free to have displacement along the X and Y directions and in constrained in the Z direction.
- Displacement of the workpiece bottom face is constrained along the Y and Z directions and a 50mm time variant displacement in X direction.
- The tool is supported by fixing the nodes on the top and back of the tool in both x and y direction.

- Varied constant cutting speed is applied on cutting tool in the X direction for different simulations.

4. Results and discussions

Table 6. Chip morphology for cutting speed 50m/min and varying rake angle.

Rake angle	Depth of cut	Type of chips formed
15	0.1	Continuous
15	0.2	Discontinuous
15	0.5	Discontinuous
0	0.1	Continuous with BUE
0	0.2	Serrated
0	0.5	Serrated
-6	0.1	Discontinuous
-6	0.2	Discontinuous
-6	0.5	Discontinuous

Table 7. Chip morphology for cutting speed 150m/min and varying rake angle.

Rake angle	Depth of cut	Type of chips formed
15	0.1	Continuous
15	0.2	Continuous
15	0.5	Discontinuous
0	0.1	Continuous
0	0.2	Serrated
0	0.5	Serrated
-6	0.1	Continuous with BUE
-6	0.2	Discontinuous
-6	0.5	Discontinuous

Table 8. Chip morphology for cutting speed 250m/min and varying rake angle.

Rake angle	Depth of cut	Type of chips formed
15	0.1	Continuous
15	0.2	Continuous
15	0.5	Continuous with BUE
0	0.1	Continuous
0	0.2	Continuous
0	0.5	Serrated
-6	0.1	Continuous
-6	0.2	Continuous
-6	0.5	Deformed

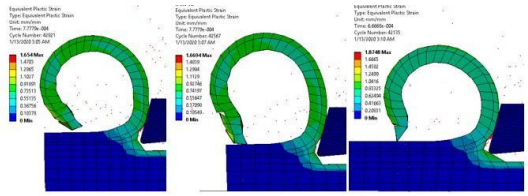

Fig 2. Comparison of chip morphology and the equivalent plastic strain distribution under the conditions of (a) v=50m/min (b) v=150m/min (c) v=250m/min, t=0.1mm, 15° rake face.

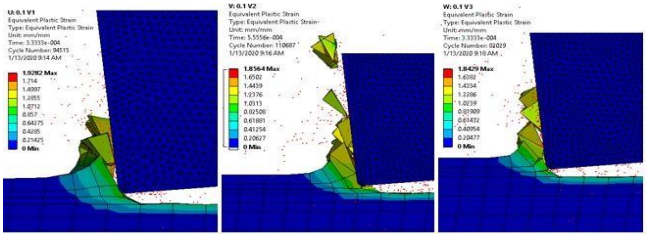

Fig. 3. Comparison of chip morphology and the equivalent plastic strain distribution under the conditions of (a) v=50m/min (b) v=150m/min (c) v=250m/min, t=0.1mm, -6° rake tool face

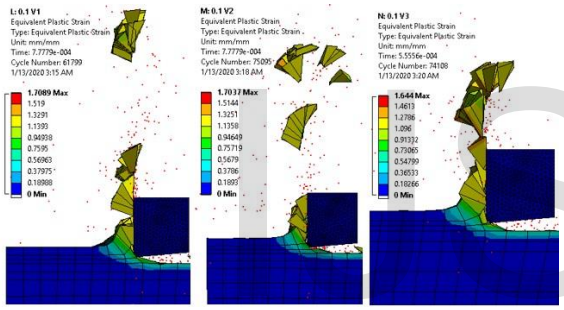

Fig. 4. Comparison of chip morphology and the equivalent plastic strain distribution under the conditions of (a) v=50m/min (b) v=150m/min (c) v=250m/min, t=0.1mm, 0° rake tool face

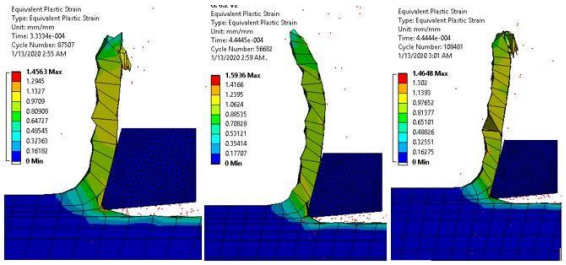

Fig 5. Comparison of chip morphology and the equivalent plastic strain distribution under the conditions of (a) v=50m/min; t=0.2mm; (b) v=150m/min; t=0.2mm; (c) v=250m/min; t=0.2mm

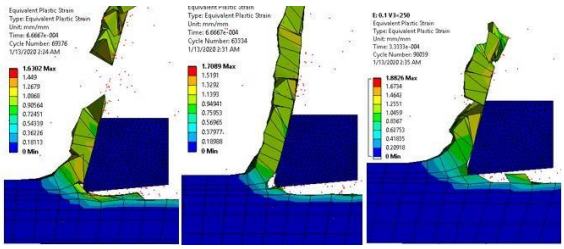

Fig 6. Comparison of chip morphology and the equivalent plastic strain distribution under the conditions of (a) v=50m/min; t=0.5mm; (b) v=150m/min; t=0.5mm; (c) v=250m/min; t=0.5mm

4.1. Effect of cutting speed on temperature distribution, chip morphology, equivalent stresses and shear stress distribution across the length of the workpiece and rake face of the tool

The cutting speed has a profound effect on the maximum temperature in the chip, as shown in Table 9 – 11, such that it is essentially proportional to the cutting speed. Inspection of Table 9 shows a steady correlation between increase in the cutting speed and rise in the maximum temperature in the cutting zone. In general, the temperature increased as the cutting speed was increased from 50m/min to 250m/min irrespective of the tool rake angle used.

Morphologies of the chips at various cutting speeds are shown in Fig. 2- 6. The observed thickness of the chips formed after the simulations are reduced at higher cutting speed, lower feed rate, and lower depth of cut. As the cutting speed increased, the chips formed become relatively ductile. Thus, the chips are increasingly in continuous form. Interestingly, at a cutting speed of 50 m/min, there is a part of chip which is continuous, and the other part has relatively different chip forms. As the cutting speed increases (150m/min), the outer surface of the chips show formation of prominent saw tooth.

profile. Further increasing to a higher cutting speed (250m/min) results in higher cutting temperatures and consequently, an increase in the ductility of the material. So, with high cutting speed, saw toothed chip sizes may get longer without breaking resulting in formation of continuous chips. The chips were found to curl as the cutting speed increases this may be due to sticking of work piece material on the tool face.

From Tables 9-11, it is shown that both the cutting and thrust forces decrease with increasing the cutting speed. Fig 8, Fig 9 and Fig 10 shows graphs that visualize the influence of the cutting speed on the cutting and thrust forces. It is observed from the table that by increasing the cutting speed from 50m/min - 250m/min, the cutting force tends to decrease. Likewise, the thrust force decreases too at higher cutting speeds. although it is not too obvious. Table 13 shows that with increasing cutting speed, the maximum value of the von mises stress distribution decreases. Although this variation in value is less than 10%. Table 14. shows the dependency of the cutting speed on the shear stress. It is observed that the tensile and compressive shear stresses fluctuate as the cutting speed was increased gradually from 50m/min to 250m/min. considering the results obtained generally, it is suspected that the greater tensile shear stresses occur between 150m/min and 250m/min.

4.2. Effect of depth of cut on the chip morphology, temperature distribution, cutting and thrust force, shear stress and von mises stresses on the workpiece

The depth of cut is also one of the influential parameters for the determination of chip type. To show the influence of the depth of cut, three different depths of cut 0.1, 0.2 and 0.5 were used.
Continuous chip without forming segmentation along the chip free edge is generated when uncut chip thickness is set to 0.2 and 0.5mm, and in contrast, the serrated chip is generated when the depth of cut is about 0.1mm under the same simulation conditions as shown in Fig. 2–6.

According to simulation results in Tables 6-8, with the increasing depth of cut, chip type tends to become more segmented and finally serrated chips are generated, that is, high depth of cut results in serrated chip while the low depth of cut results in the continuous chip. But actually, continuous chips were formed for the 0.2mm and 0.5mm depth of cut. This may be due to using very small increment in the depth of cut range and also Al 6061 material microstructure.

From Table 12, it is observed that the maximum cutting temperature rises as the depth of cut was increased. Although, this influence is latent and not as obvious as the increase in temperature due to cutting speed.

From Fig. 8- Fig. 10, plots have been made to show how the cutting and thrust forces respond to changes in both cutting speed and depth of cut. As the depth of cut was Increased, the plot shows a corresponding increase in the cutting force and thrust forces. According to the simulation results in Table 10-12, it can be concluded that as the depth of cut has a stronger influence on the cutting and thrust forces than the cutting speed, hence the depth of cut and cutting forces are essentially proportional. Closer examination of Table 13 and 14 shows that there is no significant change in the von mises stress distribution as the depth of cut increased, while the depth of cut seems have varied effect on the shear stress distribution as the shear stress. Decreased at 0.2mm and then increased back again at 0.5mm depth of cut. General observation of the results shows that the tensile shear stresses are minimum at medium speed, that is at 150m/min.

4.3. Influence of tool rake angle on the chip morphology, temperature distribution, the cutting and thrust force, the shear stress and von mises stresses on the work piece

Three different rake angles are used to study the effect of rake angle on the chip formation process. In addition, the effects of rake angle in chip formation are simulated. Generated chips tend to be serrated and eventually the discontinuous type when the tool rake angle is moving from positive values to negative values as summarized in tables 6-8. The formation of continuous, serrated and discontinuous chips was simulated by using the different tool rake angles. A continuous chip with a little segmentation is generated with a positive rake angle of 15º (Fig. 2); a serrated or saw-tooth chip is generated with a 0º rake angle tool (Fig. 5); a discontinuous chip, sometimes with two split parts is generated with a negative rake angle of –6º (Fig. 4); Obviously, the tendency from continuous to discontinuous chip formation is increasing when the rake angle is moving from positive to negative values. As a result of the negatively increasing tool rake face, compression on the chip increases. This higher compression results in tearing stress increasing in the primary shear region, which in turn promotes segmentation, and then eventually results in separation of each. Conclusively, it is seen that negative rake angles tend to produce discontinuous chips while positive angles result in continuous chip formation. Serrated chips can be obtained within the middle range of the tool rake angles.

Inspection of Table 12 shows that the variation of the maximum temperature with tool rake face angle. The simulation results show that the temperature rises in the work piece and chip increases from positive rake angle (15°) to the negative angle (-6°).

It can be seen that the forces on the rake face are slightly decreased at higher rake angles. The decrease in forces at higher rake angle can be attributed to the fact that as the rake angle increases, the chip remains on the rake of the tool for a shorter length, and the curling of the chip occurs

faster. It can be seen that as the rake angle increased from -6° to 15°, the cutting forces and thrust forces all reduced. This may be attributed to the fact that when the rake angle is positive, the cutting edge is sharp, and the cutting force and thrust force of course will be smaller, but when the rake angle is negative, the cutting edge is blunt, so the cutting force and the thrust force will be larger.

By close examination of Table 13-14 containing the maximum equivalent and shear stresses obtained from the simulation, it can be noted that shear angle increases with the increase in rake angle. The von mises (effective stress) decreases with increasing tool rake angle**.**

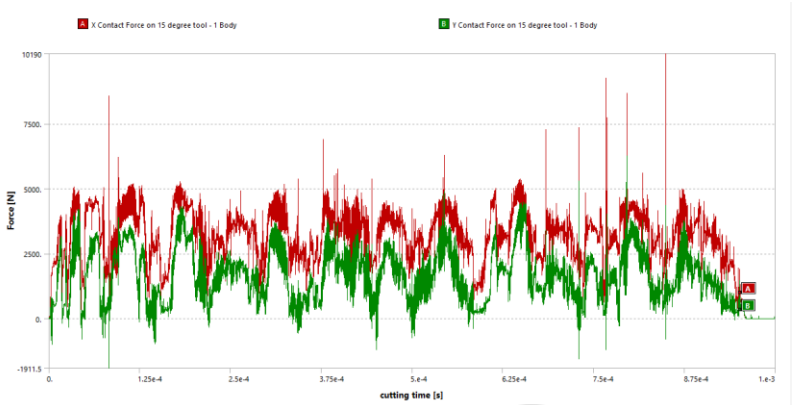

Fig. 7. Cutting and thrust force obtained from the simulation at (v = 50 m/min, t =0.1mm).

Table 9. Cutting and thrust force for cutting speed 50m/min and varying depths of cut the 15° rake tool.

Depth of cut	Cutting force			Thrust force		
Cutting speed	50m/min	150m/min	250m/min	50m/min	150m/min	250m/min
0.1	3031.98	2961.21	2897.98	2961.21	1519.01	1557.37
0.2	2728.45	2696.67	2632.09	2696.67	1245.08	1292.52
0.5	4318.41	4203.65	4150.66	4203.65	2575.53	2562.15

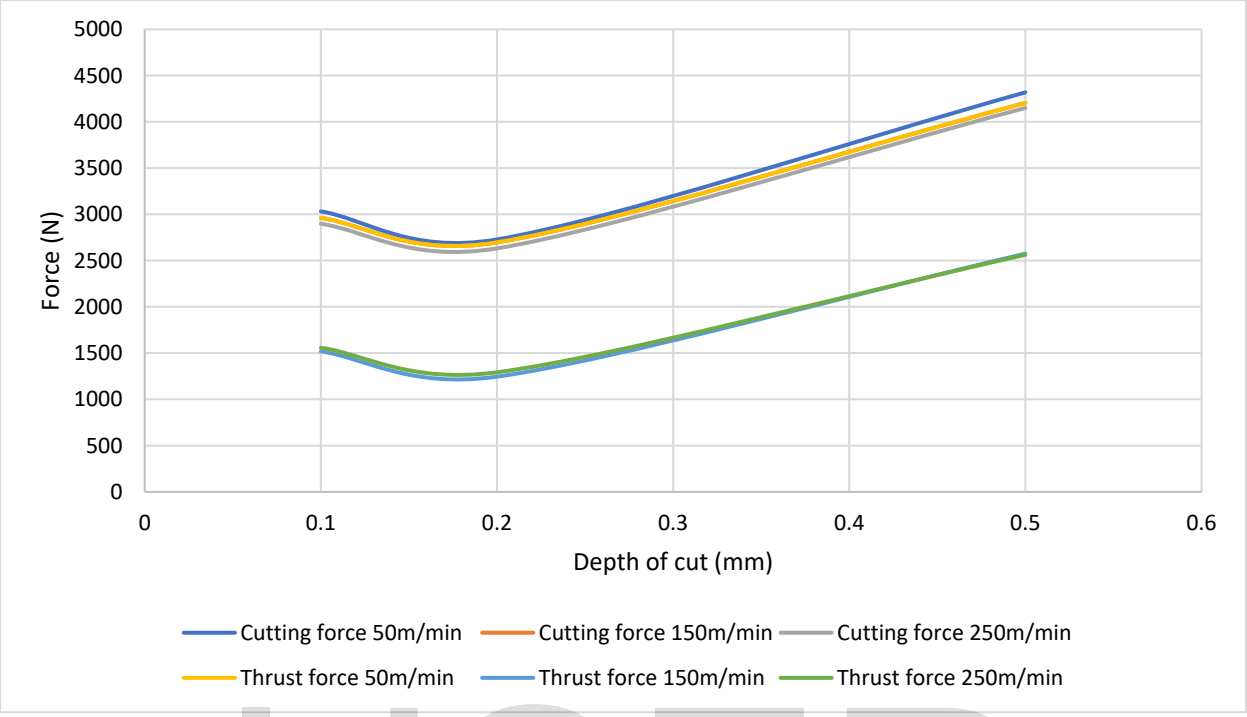

Fig. 8. Plot showing the effect of both depth of cut and cutting speed on Cutting and thrust forces of the 15° rake tool.

Table 10. Cutting and thrust force for varying cutting speed and varying depths of cut of the 0° rake tool.

Depth of cut	Cutting force			Thrust force		
Cutting speed	50m/min	150m/min	250m/min	50m/min	150m/min	250m/min
0.1	3193.74	3103.61	3098.98	1793.63	1762.05	1802.55
0.2	3231.34	3203.63	3121.35	1939.65	1927.14	1935.55
0.5	4564.52	5299.14	4373.19	2812.26	3351.08	2718.44

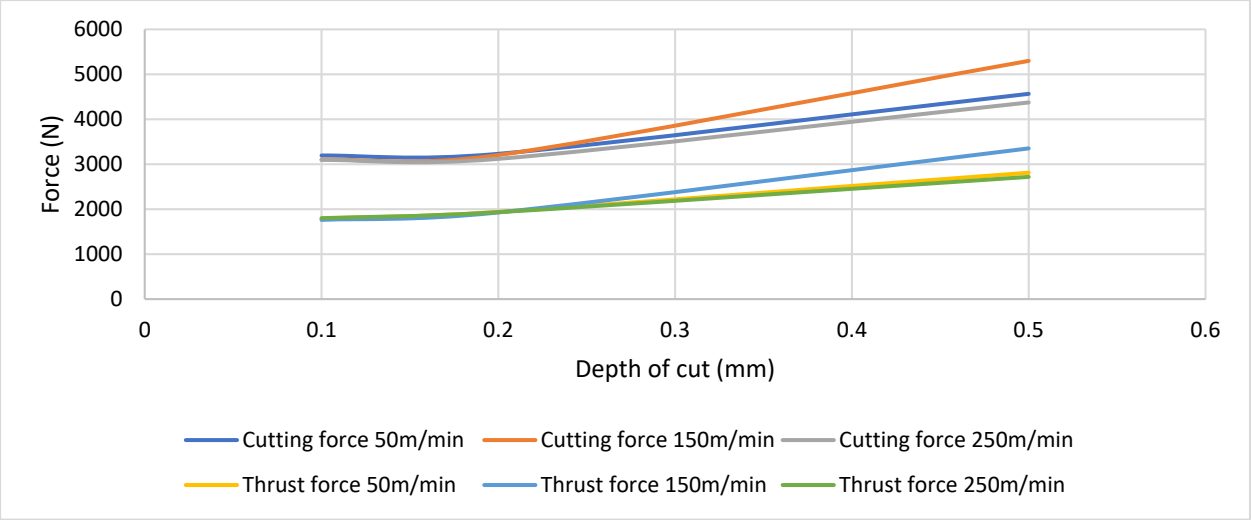

Fig. 9. Plot showing the effect of both depths of cut and cutting speed on Cutting and thrust forces 0° rake tool

Table 11. Cutting and thrust force for varying cutting speed and varying depths of cut of the -6° rake tool.

Depth of cut	Cutting force			Thrust force		
Cutting speed	50m/min	150m/min	250m/min	50m/min	150m/min	250m/min
0.1	3258.2	3235.27	3234.44	1920.51	1956.02	1846.12
0.2	3494.7	3396.84	3228.21	2217.32	2170.37	1947.35
0.5	5197.8	4722.58	4637.72	3435.79	3058.08	3016.96

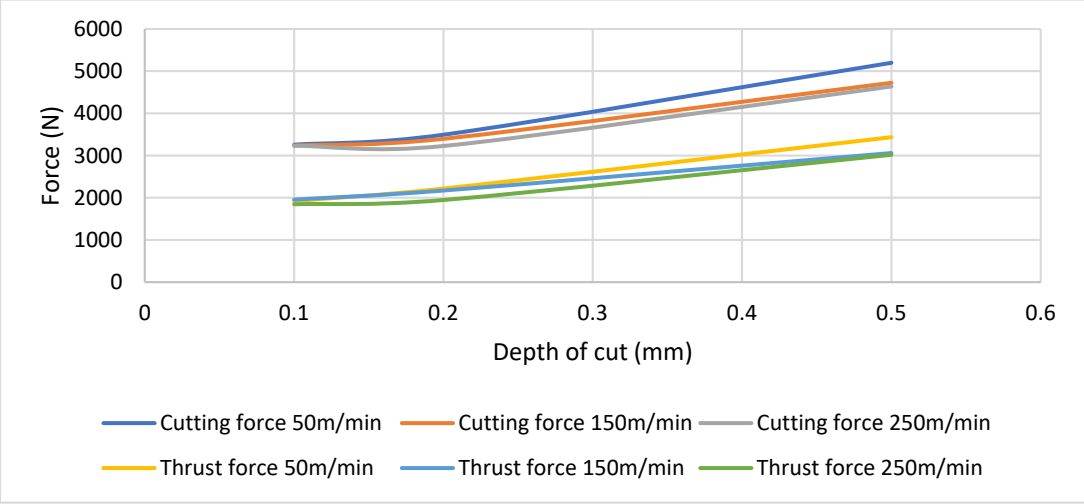

Fig. 10. Plot showing the effect of both depth of cut and cutting speed on Cutting and thrust forces -6° rake tool.

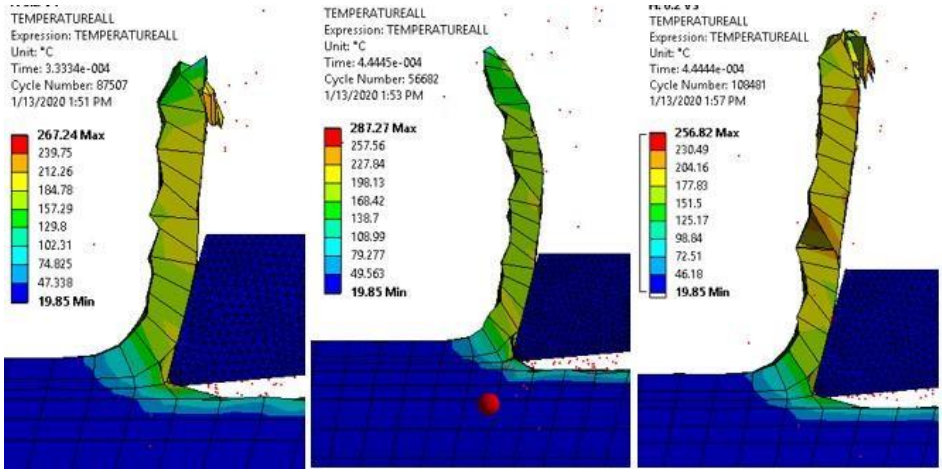

Fig. 11. Distribution of temperature in the cutting zone at t = 0.1mm, (a) v=50m/min (b) v=150m/min; (c) v=250m/min.

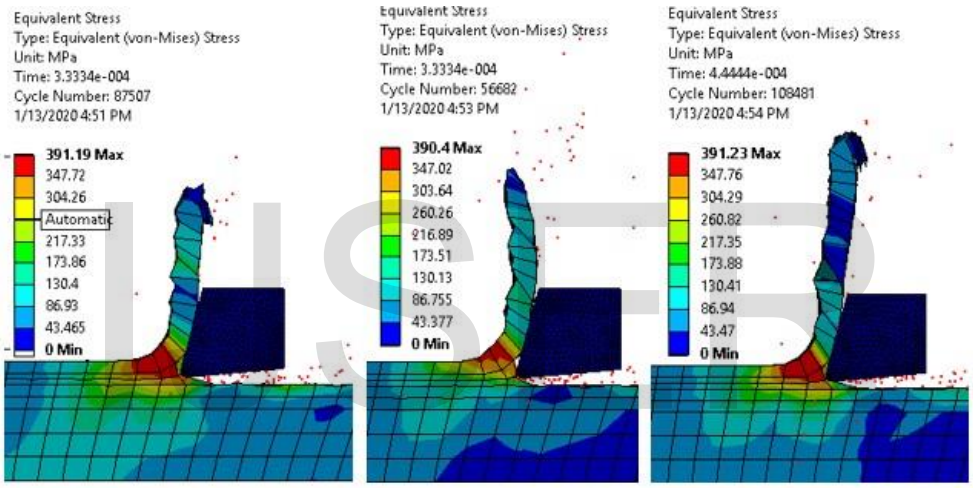

Fig. 12. Distribution of the von mises equivalent stress on the workpiece at t=0.2mm, (a) v=50m/min (b) v=150m/min; (c) v=250m/min**.**

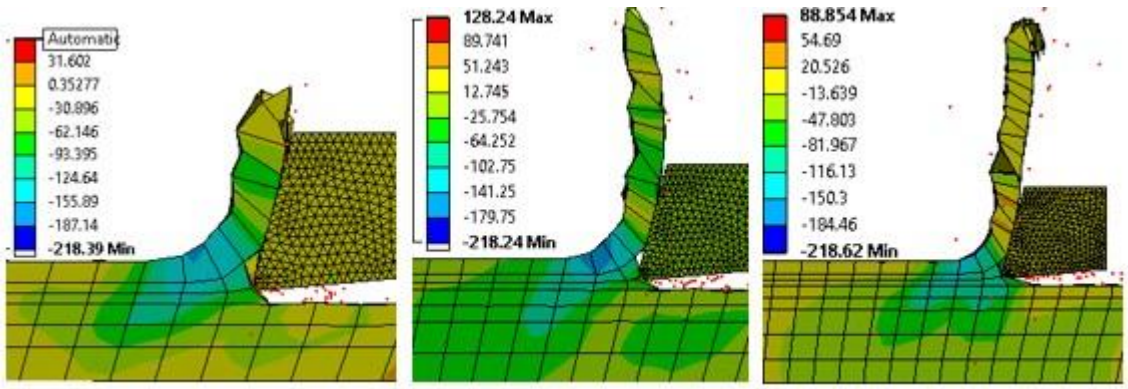

Fig. 13. Distribution of the shear stress on the workpiece at t=0.2mm, (a) v=50m/min (b) v=150m/min; (c) v=250m/min**.**

Table 12. Temperature distribution across the length of the workpiece at different cutting speeds and depth of cut (All in °C)

	15°			0°			-6°		
v	50m/min	150m/min	250m/min	50m/min	150m/min	250m/min	50m/min	150m/min	250m/min
$T_{0.1}$	**290.32**	**298.01**	**319.69**	**714.75**	**311.43**	**658.48**	**339.16**	**600.59**	**604.49**
$T_{0.2}$	**267.24**	**287.27**	**256.82**	**377.69**	**392.65**	**344.31**	**397.11**	**471.04**	**429.98**
$T_{0.5}$	**288.7**	**290.62**	**323.34**	**324.84**	**328.82**	**335.46**	**335.46**	**343.08**	**335.21**

Table 13. distribution of the maximum VON MISES equivalent stress across the length of the workpiece at different cutting speeds and depth of cut (All in MPa)

	15°			0°			-6°		
v	50m/min	150m/min	250m/min	50m/min	150m/min	250m/min	50m/min	150m/min	250m/min
$\sigma_{0.1}$	**391.36**	**388.62**	**389.96**	**391.45**	**390.38**	**388.91**	**390.80**	**389.22**	**388.54**
$\sigma_{0.2}$	**391.19**	**390.40**	**391.23**	**389.09**	**421.60**	**391.07**	**389.59**	**389.59**	**389.34**
$\sigma_{0.5}$	**389.79**	**391.36**	**389.61**	**390.06**	**390.12**	**391.03**	**388.42**	**389.42**	**389.85**

Table 14. distribution of maximum shear stress across the length of the workpiece at different cutting speeds and depth of cut (All in MPa)

	15°			0°			-6°		
v	50m/min	150m/min	250m/min	50m/min	150m/min	250m/min	50m/min	150m/min	250m/min
$\tau_{0.1}$	**137.58**	**131.92**	**108.91**	**112.06**	**97.22**	**113.60**	**146.62**	**156.13**	**148.97**
$\tau_{0.2}$	**62.851**	**128.24**	**88.85**	**202.09**	**96.97**	**96.19**	**116.18**	**123.59**	**144.21**

$\tau_{0.5}$	**201.00**	**160.88**	**200.95**	**107.68**	**111.33**	**169.80**	**33.39**	**125.68**	**147.92**

5.0 Conclusion.

As confirmed by experimental results obtained from published literature, [11], [12] and [13], our FEM simulations accurately predict chip form and allow the effects of parameters influencing chip formation to be studied. Given the material properties of the Al 6061-T6 work piece, adjusting the cutting conditions in the simulation (e.g. depth of cut, cutting speed, and tool rake angle) enables insightful prediction of the resultant chip form. It is therefore possible to predetermine the cutting parameters required to produce the serrated chip form preferred for automated machining. The Johnson-Cook model was used in combination with the Johnson-Cook damage initiation model [8], [10].

According to the results obtained from the simulations different cutting parameters, in order to improve the machined surface property, high cutting velocity, small depth of cut, and positive rake angle should be used. FEA simulation of the metal cutting process can help researchers learn more and optimize the cutting parameters to improve manufacturing efficiency and the quality of machined parts.

The models obtained by FEM have several advantages, including the eliminating material wastage and reducing time relative to actual experiments and approximates the distribution of stress, plastic strain, and temperature in the deformation zone, which can be hardly measured experimentally without getting expensive equipment, these results being in good agreement with reported results of other FEA orthogonal cutting models [15] [16] [17].
Further work: the numerical model setup in ANSYS/Explicit dynamics™ can be considered to be reliable enough to make qualitative analysis of process parameters related to the metal cutting process and tool geometry. Finite Element Modelling of chip formation process is qualitatively robust enough with regards to process parameters, however, the quantitative results need to be carefully assessed.

REFERENCES

[1] M,S Najiha, M.M Rahman, and K. Kadirgama (2015) “Machining Performance of Aluminium alloy 6061-T6 on Surface Finish using Minimum Quantity Lubrication” International Journal of Automotive and Mechanical Engineers Vol 11 pp 2699-2712.

[2] Najiha MS, Rahman MM, Yusoff AR, Kadirgama K. (2012) “Investigation of flow behaviour in minimum quantity lubrication nozzle for end milling processes”. International Journal of Automotive and Mechanical Engineering.;6:76876.
[3] Akram, S., Jaffery, S. H. I., Khan, M., Fahad, M., Mubashar, A., and Ali, L., (2018) "Numerical and Experimental Investigation of Johnson-Cook Material Models for Aluminum (Al 6061-T6) Alloy Using Orthogonal Machining Approach," Advances in Mechanical Engineering, Volume 10, No. 9, pp. 1-14.

[4] JUNAIDI dan EDDY, (2017,) "Analysis of Cutting Carbide Tools with S45C Material on Universal Lathes," in Seminar Nasional FT.UISU, pp. 116–123

[5] Sima, M. and Özel, T.,(2010) "Modified Material Constitutive Models for Serrated Chip Formation Simulations and Experimental Validation in Machining of Titanium Alloy Ti-6Al-4V," International Journal of Machine Tools and Manufacture, Volume 50, No. 11, pp. 943-960,

[6] Duan, C. Z., Yu, H. Y., Cai, Y. J., and Li, Y. Y.,(2010.) "Finite Element Simulation and Experiment of Chip Formation during High Speed Cutting of Hardened Steel," Applied Mechanics and Materials, Volume 29-32, No. 5, pp. 1838-1843,

[7]. Thi-Hoa Pham, Thi-Bich Mac, Van-Canh Tong, Tien-Long Banh and Duc-Toan Nguyen (2016), Simulation and experimental studies to verify the effect of cutting parameters on chip shrinkage coefficient and cutting forces in machining of A6061 aluminum alloy Advances in Mechanical Engineering, Vol. 8(10) 1–11

[8] Johnson, G. R. and Cook, W. H., (1983) "A Constitutive Model and Data for Metals Subjected to Large Strains, High Strain Rates and High Temperatures," 7th International Symposium on Ballistics. pp. 541-547,.

[9] Hashemi, J., Tseng, A. A., and Chou, P. C, (1994), Finite Element Modeling of Segmented Chip Formation in High-Speed Orthogonal Machining, Journal of Materials Engineering and Performance, 3, pp. 712-721.

[10] Johnson, G. R. and Cook, W. A, (1985) "Fracture Characteristic of Three Metals Subjected to Various Strains, Strain Rates, Temperatures and Pressures," Engineering Fracture Mechanics, Volume 21, No. 1, pp. 31-48,

[11] Adedeji K.A (2016)," Numerical and Experimental Investigations of Thermo-Mechanical Stress Distribution in Turning Operation"Ph.D Thesis Federal University of Agriculture Abeokuta,Nigeria.

[12] Shukry H. Aghdeab, Adil S., Mohammed J., Baqer A., Anfis (2018) "Optimization of Cutting Parameters for Mrr in Turning processes" Association of Arab Universities Journal of Engineering Sciences NO.4 Volume. 25

.

[13] Liu J, Bai Y and Xu C (2013)." Evaluation of ductile fracture models in finite element simulation of metal cutting processes". J Manuf Sci Eng; 136: 011010.

[14] B. Lan, et al (2012)., "Identification of Material Constitutive Parameters Using Orthogonal Cutting Tests and Genetic Algorithm", Materials Science Forum., 112–116.

[15] Komvopoulos, K. and Erpenbeck, S. A., (1991), Finite Element Modeling of Orthogonal Cutting, Journal of Engineering for Industry, 113, pp. 253-267.

[16] C. Hortig, B. Svendsen, Simulation of chip formation during high-speed cutting (2007), Journal of Materials Processing Technology 186: 66-77.

[17] G. Sutter, et al., (2005), Chip geometries during high-speed machining for orthogonal cutting conditions, International Journal of Machines Tools and Manufacturing 45 719726.

[18] ANSYS 19.2 Version